Optical image correlation with a binary spatial light modulator

Demetri Psaltis
Eung G. Paek
Santosh S. Venkatesh
California Institute of Technology
Department of Electrical Engineering
Pasadena, California 91125

Abstract. The use of a binary, magneto-optic spatial light modulator as an input device and as a spatial filter in a VanderLugt correlator is investigated. The statistics of the correlation that is obtained when the input image or the spatial filter is thresholded are estimated. Optical correlation using the magneto-optic device at the input and Fourier planes of a VanderLugt correlator is demonstrated experimentally.

Keywords: optical pattern recognition; spatial light modulator; correlation; matched filter; optical data processing.

Optical Engineering 23(6), 698-704 (November/December 1984).

CONTENTS

1. INTRODUCTION

Optical image correlation was originally demonstrated by VanderLugt[1] for the implementation of matched filtering. Subsequently, numerous other correlation-based recognition algorithms also have been implemented optically,[2] and it has been established that optical image correlation can be a powerful tool for pattern recognition applications. The implementation of an image correlator generally requires two spatial light modulators (SLMs), through which the input and reference images are entered in the optical system. Several SLMs have been developed for this purpose, but the lack of devices suitable for system applications remains a limitation of the technique. In this paper we investigate the possibility of using the magneto-optic device (MOD) that recently has been developed at Litton Data Systems as a SLM in optical image correlators. The MOD is a binary modulator, and therefore the question arises as to whether a binary SLM is useful for image correlation. This is one of two issues addressed in this paper. The second issue is whether the MOD is compatible with the requirements of coherent optical processors. We explore this issue through the experimental implementation of coherent image correlators using the device.

The operation and the properties of the MOD are briefly reviewed in the following section. In Sec. 3 we consider the use of this device as an input SLM. The statistical analysis of a binary image correlator and experimental implementation are included. In Sec. 4 we present and analyze the performance of a simple method for recording computer-generated Fourier transform holograms on the MOD. Correlations that were experimentally obtained optically using such computer-generated holograms (CGHs) are presented.

2. MAGNETO-OPTIC SPATIAL LIGHT MODULATOR

The principle of operation and the characteristics of the MOD have been reported in the literature recently.[3,4] The device consists of a two-dimensional array of magneto-optic modulators that are fabricated monolithically on the same nonmagnetic substrate. Presently, devices with 128×128 elements are being fabricated, and larger arrays are likely to become available in the near future. Each element of the array can be individually addressed electronically through an array of crossed electrodes. The structure of the MOD is shown schematically in Fig. 1. When current is applied to a pair of crossed electrodes, a sufficiently high magnetic field is produced at the location where the two electrodes cross so that the magnetization of the pixel at that location is aligned with the applied magnetic field. Only one of the four pixels that surround the position where each pair of electrodes cross is affected because the lower-right corner in each pixel is ion-implanted and this reduces the strength of the applied magnetic field that is required to initiate the magnetization switching. Each pixel of the array can be magnetized in a direction perpendicular to the surface in either polarity. Two pixels of the MOD, magnetized in opposite polarities, are shown in Fig. 2. The pixels are illuminated with a plane wave polarized in the y direction. The propagation of light through the magnetized medium results in a rotation of the plane of polarization by an angle θ around the z-axis due to the Faraday effect. The direction of the Faraday rotation is opposite for the two stable magnetization states, as shown in Fig. 2. The light that is transmitted through the MOD is normally viewed through an analyzer that is oriented to block one of the rotated polarizations. A portion of the incident light is transmitted through pixels that are magnetized in the opposite direction, and thus an image of the binary pattern that is stored in the MOD is observed. This method for observing the stored image provides maximum contrast and is therefore optimum for display applications. In information processing, however, we are interested in the information content. If we examine the x and y components of the two rotated polarizations in Fig.2, we realize that the y component (parallel to the incident polarization) is not affected by the magnetization state of the pixel. Thus, the portion of the transmitted light that is polarized in the y direction is unmodulated and acts as a uniform background bias. The direction (or, equivalently, the polarity) of the orthogonal, or x, component is determined by the polarity of the magnetization of the pixel. Therefore, the information that is recorded on the MOD is transferred to the x polarization only. Bipolar modulation of the light amplitude can be obtained if the MOD is used in conjunction with an analyzer oriented to transmit the x polarization. Bipolar modulation is generally desirable in optical processing systems since it eliminates the need for the bias that is typically used to represent bipolar signals.

A simple experiment was performed to demonstrate the bipolar modulation property of the MOD. A grating was recorded on a device with 48×48 pixels by magnetizing alternate columns in opposite directions. The Fourier transform and the image of this grating were optically formed for different settings of the analyzer. The results of the experiment are shown in Fig. 3. In Fig. 3(a) the analyzer was set parallel to the incident polarization. The diffraction pattern in this case is due to the pixel structure of the MOD; the pattern is

Invited Paper PR-111 received April 4, 1984; revised manuscript received May 1, 1984; accepted for publication Sept. 13, 1984; received by Managing Editor Sept. 17, 1984.
© 1984 Society of Photo-Optical Instrumentation Engineers.

Downloaded From: https://www.spiedigitallibrary.org/journals/Optical-Engineering on 28 Oct 2021
Terms of Use: https://www.spiedigitallibrary.org/terms-of-use

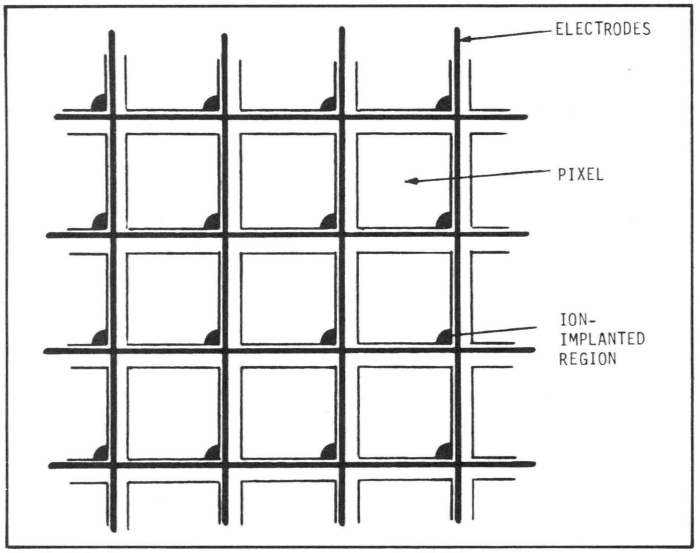

Fig. 1. Pixel structure of the magneto-optic SLM.

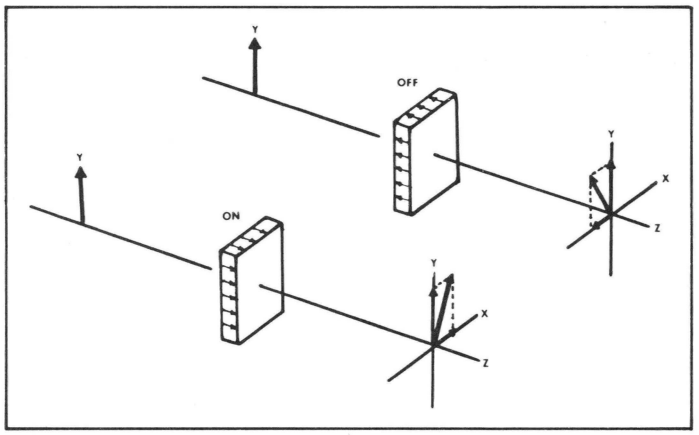

Fig. 2. Optical modulation through the magneto-optic (Faraday) effect.

symmetric in the two dimensions, indicating that the 1-D grating information is not present. The photographs in Fig. 3(b) were recorded by setting the analyzer perpendicular to the incident polarization. The diffraction pattern in this case is that of a bipolar or binary-valued phase grating. Notice that the DC component is absent in the diffraction pattern in Fig. 3(b). There is no contrast in the corresponding image in this case since the intensity of the bipolar modulation is detected. When the analyzer is set so that one of the rotated polarizations is blocked [Fig. 3(c)], the contrast is maximized in the image and the Fourier transform becomes that of a conventional amplitude grating.

3. CORRELATION OF THRESHOLDED INPUT IMAGES

A schematic diagram of the classic VanderLugt correlator is shown in Fig. 4. The implementation of this processor requires two 2-D SLMs. The input image is recorded on a SLM at plane P_1 of Fig. 4, and the Fourier transform of the reference image is holographically recorded on a second SLM at plane P_2. The correlation between the two images forms at the output plane P_3. In this section we examine the possibility of implementing the VanderLugt processor using the MOD in the input plane P_1. Since the MOD is a binary SLM, we first determine the conditions for which the use of a binary SLM is appropriate. We then experimentally investigate the suitability of this device for use in the input plane of a coherent optical correlator.

If the input image is binary and essentially noise-free (text recognition for example), then, of course, the use of a binary SLM does

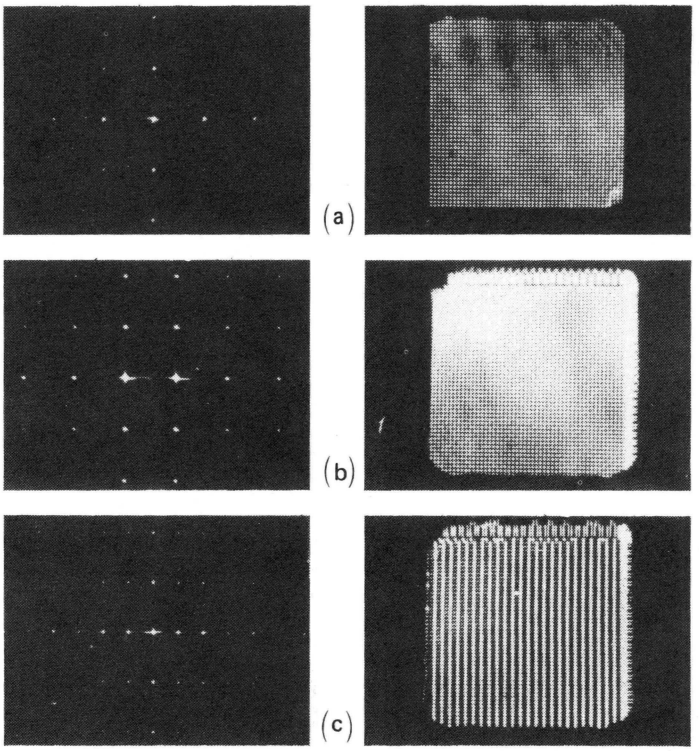

Fig. 3. Experimental demonstration of the bipolar modulation capability of the MOD.

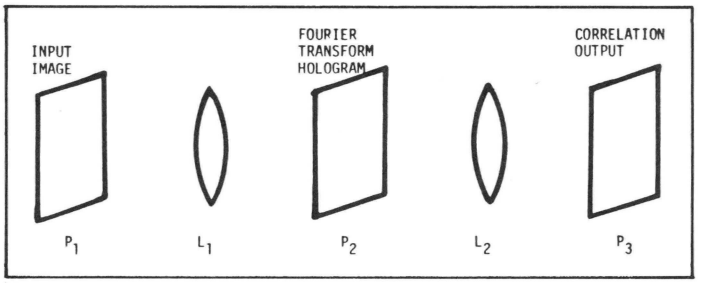

Fig. 4. VanderLugt correlator.

not present any problem. It has been shown by Kumar[5] that if the input image is not binary but is noise-free, then the performance of the correlator is not degraded if the input image is thresholded before it is correlated. Specifically, the processing gain or, equivalently, the ratio of the peak correlation value to the side-lobe level, is proportional to the square root of the space-bandwidth product of the reference in both cases.

We now investigate the effects of thresholding in the presence of additive noise. Let f(i,j) be an image we wish to recognize. We take f(i,j) to be a sample realization of a discrete sequence of independent, identically distributed Gaussian random variables with zero mean and variance σ_f^2. The input image to the correlator is the sum of f(i,j) and n(i,j), where n(i,j) is an independent, discrete sequence of Gaussian random variables with zero mean and variance σ_n^2. The thresholded input image is defined as

$$f'(i,j) = \begin{cases} 1 & \text{if } f(i,j) + n(i,j) > 0 \\ -1 & \text{if } f(i,j) + n(i,j) < 0 \ . \end{cases} \tag{1}$$

The reference image h′(i,j) is obtained by thresholding f(i,j):

$$h'(i,j) = \begin{cases} 1 & \text{if } f(i,j) > 0 \\ -1 & \text{if } f(i,j) < 0 \ . \end{cases} \tag{2}$$

Downloaded From: https://www.spiedigitallibrary.org/journals/Optical-Engineering on 28 Oct 2021
Terms of Use: https://www.spiedigitallibrary.org/terms-of-use

The correlation between the thresholded input and reference images is then given by

$$g'(i',j') = \sum_{i}^{N} \sum_{i}^{N} f'(i,j)\, h'(i+i', j+j') \ . \tag{3}$$

The expected value and the variance of the above correlation are given by the following expressions:

$$E[g'(i',j')] = \sum_{i}^{N} \sum_{j}^{N} E[f'(i,j)\, h'(i+i', j+j')] \ , \tag{4}$$

and for $(i' \neq 0, j' \neq 0)$,

$$\begin{aligned} \mathrm{var}[g'(i',j')] &= \sum_{i}^{N} \sum_{j}^{N} \sum_{i_1}^{N} \sum_{j_1}^{N} E[f'(i,j)\, h'(i+i', j+j') \\ &\quad \times f'(i_1,j_1)\, h'(i_1+i', j_1+j')] \ , \\ &= \sum_{i}^{N} \sum_{j}^{N} E[f'^2(i,j)\, h'^2(i+i', j+j')] = N^2 \ . \end{aligned} \tag{5}$$

The expected value of the product $f'(i',j')\, h'(i',j')$ can be calculated as follows:

$$\begin{aligned} &E[f'(i,j)\, h'(i+i', j+j')] \\ &\quad = 1 - 2P[f'(i,j)\, h'(i+i', j+j') = -1] = 1 - 2P_e \ , \end{aligned} \tag{6}$$

where

$$\begin{aligned} P_e &= [f'(i,j)\, h'(i+i', j+j') = -1] \\ &= \tfrac{1}{2}\{P[f(i,j) + n(i,j) > 0 \,|\, f(i+i', j+j') < 0] \\ &\quad + P[f(i,j) + n(i,j) < 0 \,|\, f(i+i', j+j') > 0]\} \\ &= P[f(i,j) + n(i,j) < 0 \,|\, f(i+i', j+j') > 0] \ . \end{aligned} \tag{7}$$

If $(i' \neq 0, j' \neq 0)$, then

$$\begin{aligned} &P[f(i,j) + n(i,j) > 0 \,|\, f(i+i', j+j') < 0] \\ &\quad = P[f(i,j) + n(i,j) > 0] = \tfrac{1}{2} \ . \end{aligned} \tag{8}$$

If $(i' = 0, j' = 0)$, then

$$\begin{aligned} P_e &= P[f(i,j) + n(i,j) > 0 \,|\, f(i,j) < 0] \\ &= \int_{0}^{\infty} \int_{x}^{\infty} P_{(f,n)}(x,y)\, dx dy \ , \end{aligned} \tag{9}$$

where

$$P_{(f,n)}(x,y) = \frac{1}{2\pi\sigma_f\sigma_n} \exp\left(\frac{-x^2}{2\sigma_f^2}\right) \exp\left(\frac{-y^2}{2\sigma_n^2}\right) \tag{10}$$

is the joint density of $f(i,j)$ and $n(i,j)$. Substitution of Eq. (10) in Eq. (9) gives the following result[6]:

$$P_e = \frac{1}{\sqrt{2\pi}\, \mathrm{SNR}_{in}} \int_{0}^{\infty} [1 - \phi(x)] \exp\left[\frac{-x^2}{2(\mathrm{SNR}_{in})^2}\right] dx \ , \tag{11}$$

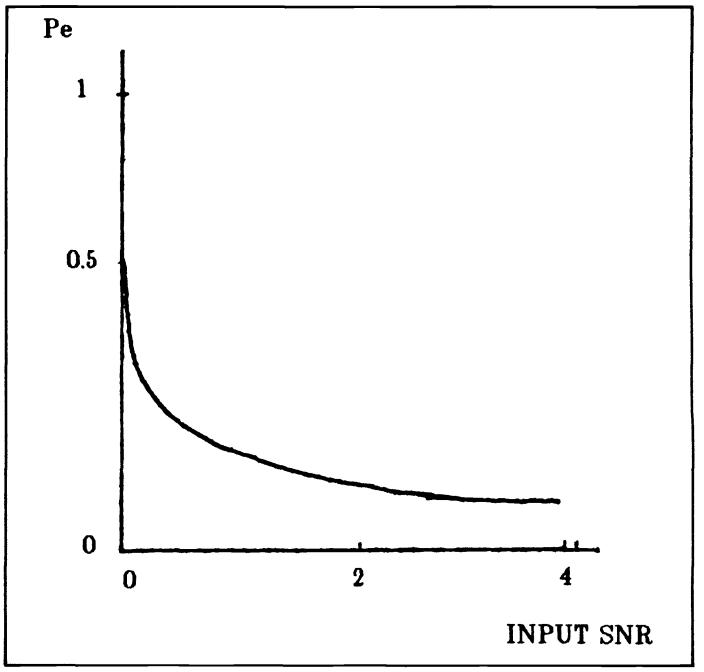

Fig. 5. Probability of misclassification of a single pixel as a function of input SNR.

where

$$\phi(x) = \int_{-\infty}^{x} \exp\left(\frac{-y^2}{2}\right) dy \ , \tag{12}$$

$$\mathrm{SNR}_{in} = \frac{\sigma_f}{\sigma_n} \ . \tag{13}$$

The integral in Eq. (11) does not have a closed-form solution, but it can easily be evaluated numerically. P_e versus SNR_{in} is plotted in Fig. 5. We now express the expected value of the correlation function $g'(i',j')$ in terms of P_e. Substituting Eqs. (6), (8), and (11) in Eq. (4), we obtain

$$E[g'(i',j')] = \begin{cases} N^2(1-2P_e) & \text{if } (i'=0, j'=0) \\ 0 & \text{otherwise} \ . \end{cases} \tag{14}$$

The ratio of the square of the correlation peak to the variance away from the peak (side-lobe level) is

$$\mathrm{SNR}' = \frac{E^2[g'(0,0)]}{\mathrm{var}[g'(i',j')]} = N^2(1-2P_e)^2 \ . \tag{15}$$

In order to appreciate the effects of thresholding, we compare this ratio with the signal-to-noise ratio that is obtained if the input image is not thresholded before the correlation. It can be easily shown[5] that in this case

$$\mathrm{SNR} = \frac{E[g(0,0)]}{\mathrm{var}[g(i',j')]} = \frac{N^2 \mathrm{SNR}_{in}^2}{1 + \mathrm{SNR}_{in}^2} \ . \tag{16}$$

The two ratios, SNR′ and SNR, are plotted in Fig. 6 as a function of SNR_{in}^2. Notice that the output SNR is larger for low input SNR when thresholding is used. Both ratios asymptotically converge to N^2 as the input SNR gets large. The SNR of the correlation of the

Downloaded From: https://www.spiedigitallibrary.org/journals/Optical-Engineering on 28 Oct 2021
Terms of Use: https://www.spiedigitallibrary.org/terms-of-use

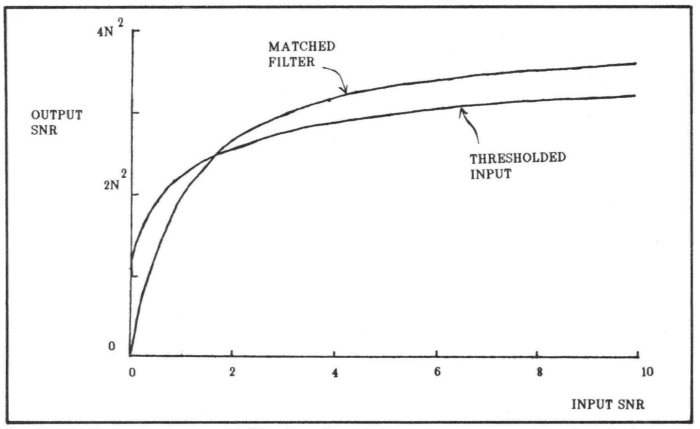

Fig. 6. Output vs input SNRs for the binary and conventional correlators.

thresholded image, however, increases at a lower rate with SNR_{in}, and thus there is a crossover at approximately $SNR_{in} = 2$. At this point, the output SNR exceeds $N^2/2$ (one-half of the number of pixels of the input image), and thus the loss in output SNR for $SNR_{in} > 2$ will not degrade appreciably the probability of detection in a typical application in which N^2 is a large number.

The conclusions we can draw from this analysis are that, under the stated assumptions, thresholding the input image before it is applied to the correlator actually improves the performance if the input SNR is low and that the performance is only marginally degraded if the input SNR is high (in which case the performance of the correlator is limited by the side-lobe level). The assumptions used in the analysis are that the input image and the additive noise are both uncorrelated. Kumar[5] has shown that in the absence of additive noise the performance is only marginally degraded if the input image is assumed to be a sample realization of a correlated noise process. The remaining case to consider is the one in which the additive noise is also correlated. It can be shown that in this case the performance can be seriously degraded unless adaptive thresholding is used. A treatment of adaptive thresholding is beyond the scope of this paper, but the cases considered demonstrate that there is a broad range of problems for which thresholding before performing the correlation is acceptable or even preferable. We now turn our attention to the optical implementation of a binary correlator using the MOD as an input SLM.

The text shown in Fig. 7(a) was recorded on a MOD with 128×128 pixels and used as the input object to a VanderLugt correlator. The word "garnet," which appears four times in the text, was chosen as the reference image. Fourier transform holograms of the word "garnet" recorded on the MOD were recorded on high resolution photographic plates. The optical reconstruction of one of these holograms is shown in Fig. 7(b). This hologram was formed by setting the analyzer so that the transmittance of the MOD was effectively unipolar, and relatively low spatial frequencies were emphasized when the hologram was recorded in order to maximize the overall diffraction efficiency. The correlation shown in Fig. 7(c) was obtained by placing this hologram at the Fourier plane of the VanderLugt correlator and the MOD at the input plane using a 5 mW HeNe laser source. A strong autocorrelation peak is obtained for every occurrence of the word "garnet" in the input object, but there are also several cross-correlation peaks and a high overall background level. It is known that the performance can be improved (the cross-correlation suppressed) by constructing the hologram to emphasize the spatial frequencies that correspond to the most distinctive features of the object.[7] A second hologram was constructed from a unipolar recording of the word "garnet," and in this case relatively high spatial frequency components of the object were emphasized. The reconstruction of this hologram and the corresponding correlation pattern are shown in Figs. 7(d) and 7(e), respectively. It is evident from Fig. 7(e) that the performance improves by high spatial frequency enhancement. An even more dramatic

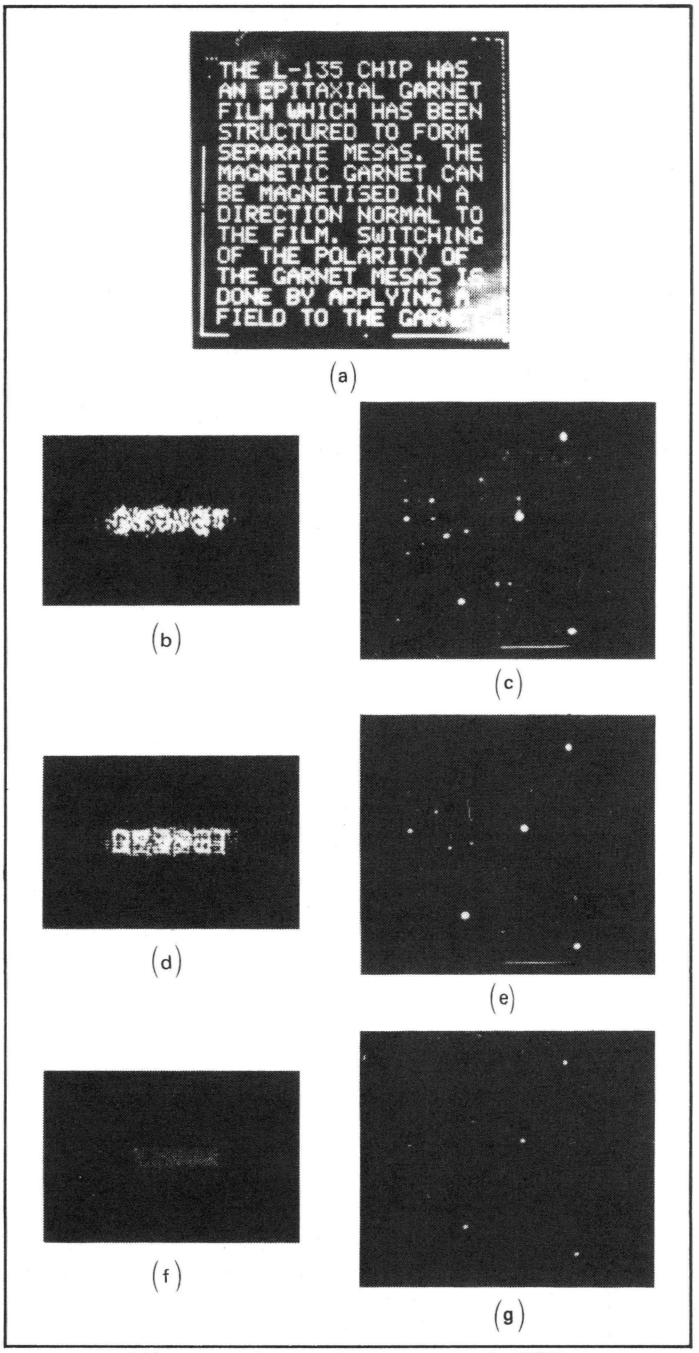

Fig. 7. Optical binary correlation experiment using the MOD.

improvement was obtained with a hologram formed from a bipolar object. The power spectrum of the bipolar object is relatively flat (the DC component is suppressed), and this allows a broader range of spatial frequencies to be holographically recorded. The image of the object is not visible in the reconstruction of the hologram of the bipolar object, shown in Fig. 7(f), since the intensity of the reconstructed image was recorded, but the sharp reproduction of the pixel structure indicates that the object has been recorded with high fidelity. The cross-correlations are very effectively suppressed in the correlation pattern shown in Fig. 7(g), except for the cross-correlation between the similar words "garnet" and "magnet." The improvement in performance is partially due to the fidelity with which the bipolar object was recorded, but it is also due to the fact that both the input and reference images in this case are bipolar and, thus, the correlation function averages very effectively to zero, except in places where there is a match between the two images. The

Downloaded From: https://www.spiedigitallibrary.org/journals/Optical-Engineering on 28 Oct 2021
Terms of Use: https://www.spiedigitallibrary.org/terms-of-use

width of the correlation peaks in Fig. 7(f) is approximately equal to the width of one pixel of the MOD.

In conclusion, we have shown that thresholding an input image before it is correlated results in an output SNR that is comparable to that obtained with a conventional correlator in many cases of interest. Therefore, a binary SLM can be used as an input device in a VanderLugt processor for a broad range of applications. Furthermore, the experiments we have presented in this section indicate that the properties of the MOD are in general compatible with the stringent requirements of a coherent optical processor; the ability to remove the DC component of the input image with polarizers rather than spatial filters is a particularly convenient property of this device.

4. IMAGE CORRELATION WITH BINARY FOURIER TRANSFORM HOLOGRAMS

We now consider the possibility of recording computer-generated Fourier transform holograms on the MOD for use in the frequency plane of a VanderLugt processor. CGHs typically are recorded as binary transparencies, and therefore the binary nature of the MOD does not in itself present a problem. The space-bandwidth product of presently available devices, however, is limited to 128×128 pixels, and thus it is important to find algorithms for constructing CGHs that require as few pixels as possible to represent each sample of the Fourier transform. Let

$$H(u,v) = |H(u,v)| \exp[j\phi_h(u,v)] = \iint h(x,y) \exp[-j2\pi(ux+vy)]\,dxdy \tag{17}$$

be the Fourier transform of the reference image $h(x,y)$. $H(u,v)$ is in general complex, and it is typically represented on a CGH by recording its magnitude using pulse width modulation and by recording its phase using pulse position modulation.[8,9] Both encoding methods consume space-bandwidth product; at least 8^2 or 16^2 samples are commonly used to represent each sample of the Fourier transform. If such an algorithm is used to record CGHs on the MOD, then images with only 16×16 or 8×8 samples can be accommodated. CGHs that require only one pixel per sample can be formed according to the following equation:

$$H'(u,v) = \operatorname{sgn}[\cos\phi_h(u,v)] = \begin{cases} +1 & \text{if } \operatorname{Re}[H(u,v)]>0 \\ -1 & \text{otherwise} . \end{cases} \tag{18}$$

$H'(u,v)$ is the transmittance of the CGH. This method permits the recording of CGHs of images with 128×128 samples on currently available MODs, but it obviously does not retain all the information in $H(u,v)$; the imaginary part of H is completely ignored and the real part is thresholded. In the following we examine the consequences of this information loss. The correlation $g(x,y)$ is obtained by recording $H'(u,v)$ on the MOD and placing it at plane P_2 of the system shown in Fig. 4 and placing a transparency of an input object $f(x,y)$ at the input plane P_1.

The correlation $g(x,y)$ is equal to

$$g(x,y) = \int_{-v_1}^{v_1}\int_{-v_2}^{v_2} F(u,v)\,H'(u,v)\exp[j2\pi(ux+vy)]\,dudv$$

$$= \iint F_r(u,v)\,H'(u,v)\exp[j2\pi(ux+vy)]\,dudv + \iint F_i(u,v)\,H'(u,v)\exp[j2\pi(ux+vy)]\,dudv , \tag{19}$$

where $F(u,v)$ is the Fourier transform of $f(x,y)$, $F_r(u,v)$ and $F_i(u,v)$ are its real and imaginary parts, respectively, and $4v_1v_2$ is the two-dimensional bandwidth of the correlator. If the input and reference images match, i.e., if $F(u,v) = H(u,v)$, then the first term in the above summation becomes

$$\int_{-v_1}^{v_1}\int_{-v_2}^{v_2} |F_r(u,v)| \exp[j2\pi(ux+vy)]\,dudv ,$$

which is the Fourier transform of a real, positive quantity and will therefore have a strong correlation peak at $(x=0, y=0)$. This occurs if and only if $F=H$, and therefore this type of hologram can be used for recognition in a manner similar to the matched filter. The expected value of the second term in Eq. (19) is zero, and its variance will be calculated shortly. The SNR that can be obtained with $H'(u,v)$ is upper-bounded by the SNR obtained with a matched filter $[H^*(u,v)]$, which is known to be the optimum linear filter. In the following we estimate the loss in SNR that results from the use of the suboptimum filter defined in Eq. (18). We assume the input image to be in the form $f(x,y) = s(x,y) + n(x,y)$, where $n(x,y)$ is a white, Gaussian process with zero mean and variance equal to σ_n^2 and $s(x,y)$ is the image to be recognized. We take $s(x,y)$ to be a sample realization of a white, Gaussian process, independent of $n(x,y)$, with zero mean and variance σ_s^2. The reference image $h(x,y)$ is set equal to $s(x,y)$ in the region $-\omega_1 < x < \omega_1$, $-\omega_2 < y < \omega_2$ and zero outside this region. The SNR of the correlation $g(x,y)$, defined in Eq. (19), is equal to

$$\operatorname{SNR}(x,y) = \frac{E^2[g(0,0)]}{\operatorname{var}[g(x,y)]} , \tag{20}$$

where[10]

$$E[g(0,0)] = \left(\frac{4\omega_1\omega_2v_1^2v_2^2\sigma_s^2}{\pi}\right)^{1/2} \int_{u=-1}^{1}\int_{v=-1}^{1} \sigma_R(u,v)\,dvdu, \tag{21}$$

and

$$\operatorname{var}[g(\omega_1x,\omega_2y)] = 4v_1v_2\sigma_n^2 + \frac{4\omega_1\omega_2v_1^2v_2^2\sigma_s^2}{\pi} \times \int_{u=-1}^{1}\int_{v=-1}^{1}\int_{u'=-1}^{1}\int_{v'=-1}^{1} 2f(u-u',v-v') \times \sin^{-1}[r(u,v,u',v')] + \sigma_R(u,v)\,\sigma_R(u',v') \times \{[1-r^2(u,v,u',v')]^{1/2}-1\} \times \exp\{i2\pi[(u-u')\,\omega_1v_1x + (v-v')\,\omega_2v_2y]\} \, dv'du'dvdu , \tag{22}$$

where

$$f(u,v) \triangleq \operatorname{sinc}(2\omega_1v_1u)\operatorname{sinc}(2\omega_2v_2v) , \tag{23}$$

$$\sigma_R(u,v) = [1+f(2u,2v)]^{1/2} , \tag{24}$$

$$r(u,v,u',v') = \frac{f(u-u',v-v')+f(u+u',v+v')}{\sigma_R(u,v)\,\sigma_R(u',v')} . \tag{25}$$

The variance consists of the sum of two terms. The first term is due

Downloaded From: https://www.spiedigitallibrary.org/journals/Optical-Engineering on 28 Oct 2021
Terms of Use: https://www.spiedigitallibrary.org/terms-of-use

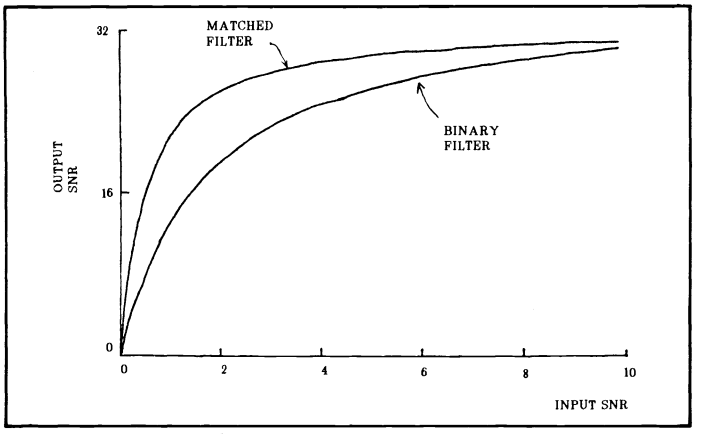

Fig. 8. Output vs input SNRs for a correlator with a binary spatial filter. The SNR of the conventional correlator is also plotted for comparison.

to the additive noise at the input, and the second term represents the energy of the side lobes in the correlation of the image s(x,y). If $\sigma_n \gg \sigma_s$, then the second term can be neglected, and Eq. (20) reduces to

$$\mathrm{SNR} = \frac{16 v_1 v_2 \omega_1 \omega_2}{\pi} \left(\frac{\sigma_s}{\sigma_n}\right)^2, \tag{26}$$

which is equal to the input SNR multiplied by the space-bandwidth product of the correlator divided by pi. Recall that the conventional matched filter enhances the SNR by the space-bandwidth product. Thus, the quantized hologram provides processing gain that is only a factor of pi less than the optimum matched filter. When the noise is sufficiently low ($\sigma_n \ll \sigma_s$), the output variance is dominated by the variance of the side lobes. The integral in Eq. (22) is difficult to evaluate numerically, particularly at high values of $v_1 v_2 \omega_1 \omega_2$, because the argument of the integral oscillates very rapidly. It is also difficult to make even an approximate analytical prediction for the value of the integral. Numerical evaluations for low space-bandwidth product indicate that the performance of the binary filter, while always slightly inferior to that of the matched filter, approaches the performance of the matched filter as the input SNR becomes large. The output SNR versus the input SNR for the binary and matched filters for a space-bandwidth product equal to 32 is plotted in Fig. 8. Experimental evidence supports this result for higher space-bandwidth products. The digitally computed correlations of a sample realization of a Gaussian random sequence with 256 samples using both a conventional matched filter and a binary filter are shown in Fig. 9. The average side-lobe level is of the same order in both cases. We therefore conclude that the binary filter is inferior to the matched filter in terms of suppressing additive noise (by a factor of pi), whereas the side-lobe level of the correlation is approximately equal in both cases.

Image correlation using the binary filter was also demonstrated experimentally with an optical system using the MOD. A CGH of the letter "O" was recorded according to Eq. (18) on a 128×128 MOD. A photograph of the hologram is shown in Fig. 10(a), and its optical reconstruction is shown in Fig. 10(b). An interesting feature of this hologram is that the primary reconstruction appears on-axis. This happens because the transmittance of this CGH is real and bipolar (not complex), and since bipolar signals can be directly recorded on the MOD, it is not necessary to record the hologram on a high spatial frequency carrier. The reconstruction is of remarkably good quality considering the extreme quantization that is involved in Eq. (18). Multiple diffracted orders are observed due to the sampling by the pixels of the MOD. Notice that the size of the higher orders does not

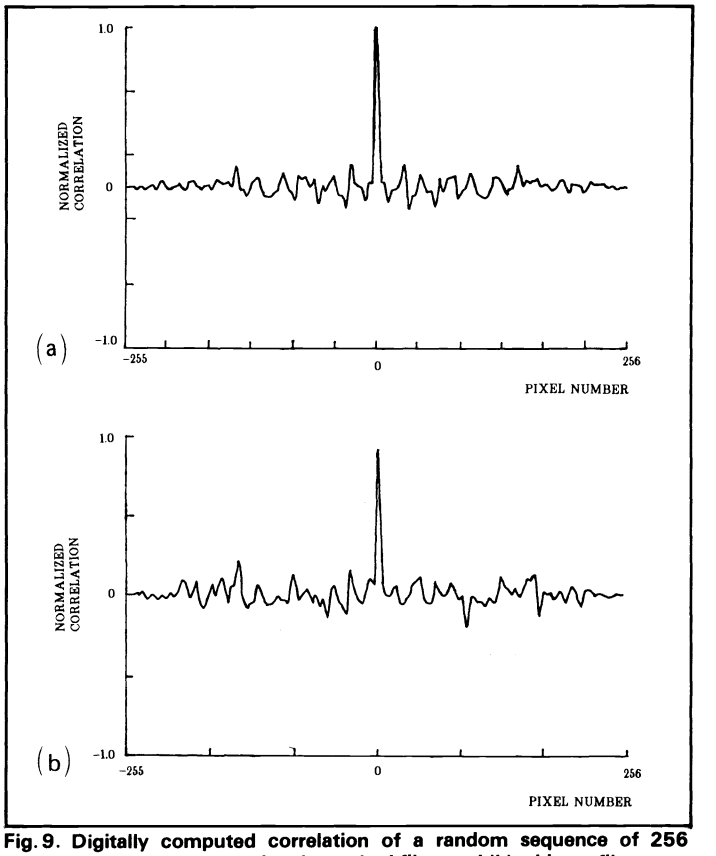

Fig. 9. Digitally computed correlation of a random sequence of 256 samples using (a) a conventional matched filter and (b) a binary filter.

increase, as is the case in conventional computer-generated holography. This is a consequence of the fact that the hologram in this case is formed at baseband. The hologram of Fig. 10 was placed at the Fourier plane of a VanderLugt system, and a transparency of the object shown in Fig. 11(a) was placed at the input plane. The transparency used in the experiment was approximately 1 cm×1.5 cm, and the focal length of the Fourier transform lens was 200 mm. The correlation shown in Fig. 11(b) was obtained using a 5 mW HeNe laser. A strong autocorrelation peak is obtained for each occurrence of the letter "O" in the input pattern; weaker spurious peaks due to the sampling in the hologram are also obtained. The value of the correlation function away from the peaks is at a comfortably low level; no attempt was made to compare the background level obtained here with that of the ideal matched filter. A considerable degree of space variance was observed, which we attribute partially to the sensitivity of the MOD to the angle of incidence of the illuminating light. The space variance limits the size of the input transparency. In our experiment we obtained satisfactory results over a 4 cm^2 area at the input plane using a Fourier transform lens with a 200 mm focal length. This experiment supports the results of our earlier analysis that a binary spatial filter can provide satisfactory performance, but it also demonstrates that the MOD has sufficient phase uniformity to be used as a holographic optical element.

5. CONCLUSION

We have examined the possibility of using a binary SLM at the input or frequency planes of a VanderLugt correlator, and we have studied how the output SNR is affected by thresholding the input or the spatial filter. In all the cases we studied we found that thresholding does not seriously degrade the performance, and in some instances the performance actually improves. We also have investigated experimentally the MOD as a candidate binary SLM with which the

Downloaded From: https://www.spiedigitallibrary.org/journals/Optical-Engineering on 28 Oct 2021
Terms of Use: https://www.spiedigitallibrary.org/terms-of-use

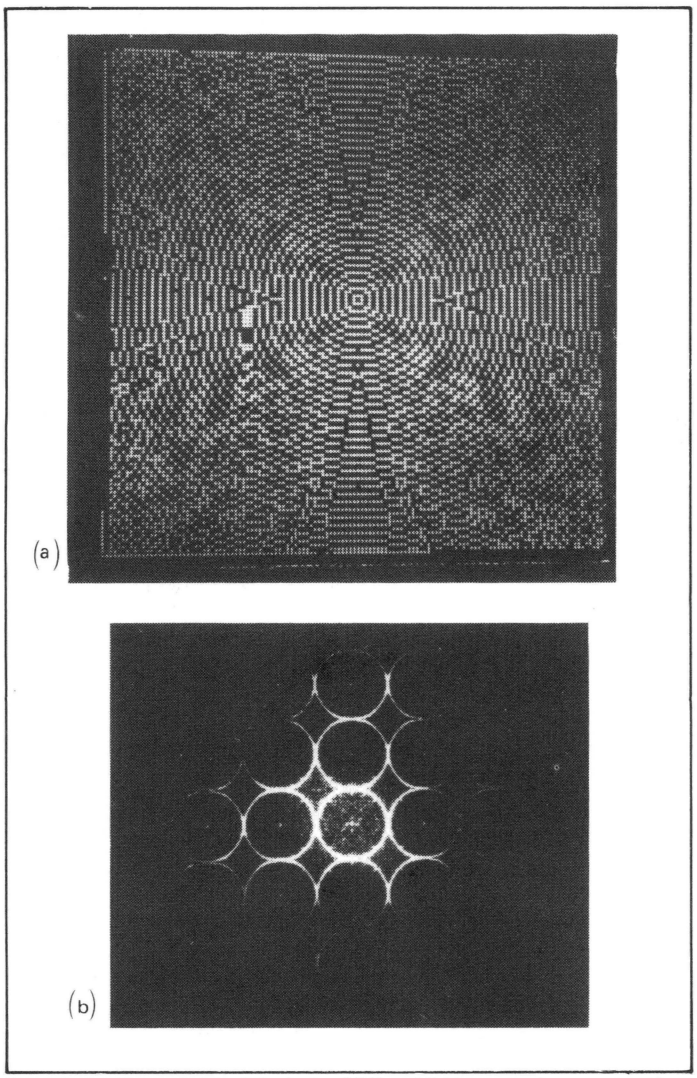

Fig. 10. (a) Binary CGH of the letter "O" and (b) its optical reconstruction.

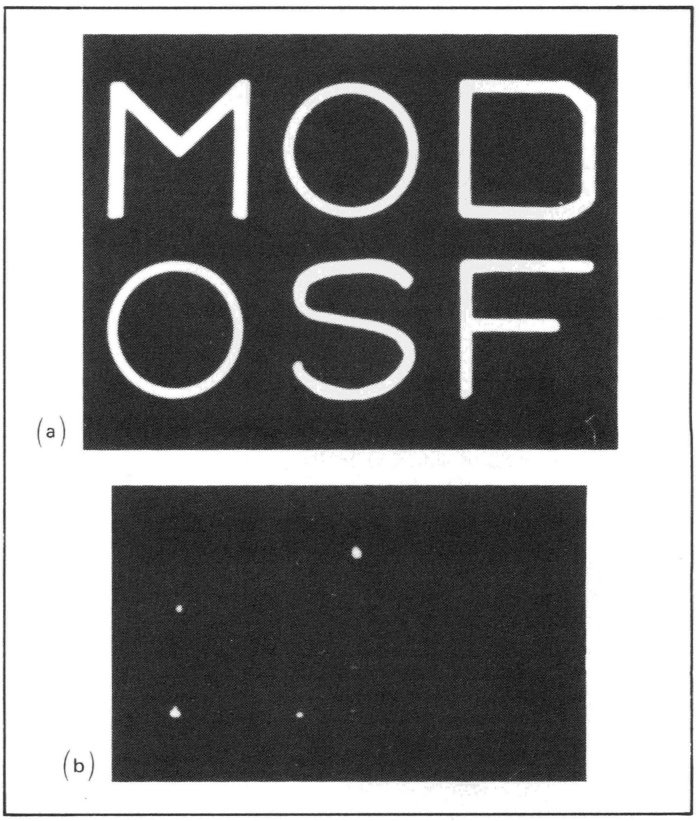

Fig. 11. Optical correlation using the binary hologram of Fig. 10.

binary correlation is optically implemented. The performance obtained with the device was generally satisfactory; its bipolar modulation capability was particularly useful in the synthesis of CGHs and in the use of the device as an input SLM. An optical image correlator with MODs at both the input and frequency planes is also possible. A potential difficulty with such an implementation is the overall light efficiency (2 to 3% for each device). A possible extension of this work is the use of the binary correlators described here for processing digitized images with more than one bit of accuracy. A separate binary correlator can be used to correlate the individual bit planes of the digitized images, and the partial correlations then can be added to produce the overall multiple-bit, 2-D correlation.[11]

6. ACKNOWLEDGMENTS

The devices used in the experiments were loaned to us by Litton Data Systems. The assistance of the technical staff at Litton, specifically W. Ross, K. Snapp, D. Fox, and R. Anderson, during this project was crucial to the experiments. We also thank F. Mok for the formation of the CGH that was used in one of the experiments. This research was supported in part by the Army Research Office.

7. REFERENCES

1. A. B. VanderLugt, IEEE Trans. Inf. Theory IT-10, 139 (1964).
2. H. J. Caulfield, R. Haimes, and D. Casasent, Opt. Eng. 19(2), 152 (1980).
3. G. R. Pulliam, W. E. Ross, B. E. MacNeal, and R. F. Bailey, J. Appl. Phys. 53, 2754 (1982).
4. W. E. Ross, D. Psaltis, and R. H. Anderson, Opt. Eng. 22(4), 485 (1983).
5. B. V. K. V. Kumar, "Coherent Optical Processing of Passive Signals," Ph.D. Thesis, Carnegie-Mellon University (1980).
6. A. Papoulis, *Probability, Random Variables, and Stochastic Processes,* McGraw-Hill, New York (1965).
7. D. Casasent and A. Furman, Appl. Opt. 17, 1652 (1978).
8. A. Lohmann and D. P. Paris, Appl. Opt. 6, 1739 (1967).
9. W. H. Lee, Appl. Opt. 18, 3661 (1979).
10. S. Venkatesh and D. Psaltis. To be published.
11. D. Psaltis, F. Mok, and E. G. Paek, in *Spatial Light Modulators and Applications,* Uzi Efron, ed., Proc. SPIE 465, 29 (1984).

Downloaded From: https://www.spiedigitallibrary.org/journals/Optical-Engineering on 28 Oct 2024
Terms of Use: https://www.spiedigitallibrary.org/terms-of-use